Manuscript 4960-Revision 1

Possible new Ca-REE-Bi phosphate minerals from a tungsten-rich calcsilicate skarn, Sierra Nevada Mountains, California

Beverly J. Berekian[1], Diane Clemens-Knott[2*], and Chi Ma[3]

[1] Geology Department, Cypress Community College, 9200 Valley View St, Cypress, CA 90630, U.S.A.
[2] Department of Geological Sciences, California State University, Fullerton, 800 N. State College Blvd., Fullerton, CA 92831, U.S.A.
[3] Division of Geological and Planetary Sciences, California Institute of Technology, Pasadena, CA 91125, U.S.A.

ABSTRACT

Scanning electron microscope and electron microprobe analyses of 3 to 15 μm diameter grains present within a garnet-quartz granofels from a tungsten skarn reveal the possible existence of at least two new rare earth element (REE)-bearing phosphate phases: $Ca(Ce,La,Bi,Nd)_2[(P,As)O_4]_2(OH)_2$ and $Ca(La,Ce,Nd,Pr,Bi)_2[(P,As)O_4]_2(OH)_2$. The analyzed REEs constitute up to 50 wt% of the phases; bismuth oxide contents range from 4.1 to 16.1 wt%. Structural data has proved impossible to obtain from these tiny grains, presumably due to radiation damage by thorium decay. These potentially new phosphate minerals are present within alteration assemblages of REE-rich epidote crystals, as well as along grain boundaries and cracks cross-cutting the quartz-garnet host rock. Association with the zeolite brewsterite-Ba suggests that these hydroxyl phosphates formed during water-rich, low temperature, retrograde mineralization in the skarn environment.

Keywords: phosphate mineral, rare earth element, bismuth, Sierra Nevada, tungsten, skarn

---

*E-mail: dclemensknott@fullerton.edu

INTRODUCTION

A detailed mineralogic examination of samples collected from a small tungsten mine in the western foothills of the Sierra Nevada Mountains in California reveals the possible presence of a variety of new minerals. In particular, distinct phosphate phases containing various abundances of the REE, bismuth and hydroxyl appear to coexist along grain boundaries and cracks, as well as within alteration assemblages replacing epidote cores (Berekian 2008). Structural data has proven impossible to collect; moreover, the collection of high quality chemical data is challenged by the small grain size (<15 μm). In this paper we present chemical data that may help define two new REE-rich phosphate phases. REE-phosphates include monazite, xenotime and varieties of apatite (Pan and Fleet 2002; Spear and Pyle 2002); naturally occurring bismuth-bearing phosphates have also been identified. REE-bearing calcium-bismuth-phosphors have been synthesized (Jiao et al., 2013) but naturally occurring REE-bearing phosphates having high bismuth contents are currently unknown.

Calcsilicate-hosted skarns are scattered throughout the Sierra Nevada batholith, having formed where Mesozoic arc plutons intruded Neoproterozoic to early Mesozoic carbonate rocks present along the southwestern margin of Laurentia (Newberry 1980, 1998). Skarn formation is characterized by an initial period of prograde metamorphism to temperatures of ~400-650ºC (Stage 1); a period of thermal equilibration between host rock and intruding pluton (Stage 2); followed by retrograde mineralization (Stage 3) marked by the invasion of meteoric and/or metamorphic fluids that promote cooling and the precipitation of metals (Einaudi et al. 1981; Corbett and Leach 1998). Some Sierra Nevada skarns host ore deposits that have proven to be economically viable, most significantly the Pine Creek mine from which more than 16 million tons of tungsten-bearing ore (0.6% WO_3) and 31 thousand tons of molybdenum and copper were

extracted (Newberry 1982; Kurtak 2007). Sierra Nevada skarns were first mined for tungsten during WWI, with production resuming during both WWII and the Korean War (Krauskopf 1953; Newberry 1980). Production in Sierra Nevada skarns continued at decreased levels until 1990 when cheaper, foreign sources of tungsten became available (Kurtak 2007).

The Consolidated Tungsten Mine (CTM), located in the western foothills near the northern edge of Tulare Co., produced ~17 thousand tons of tungsten-bearing ore (~2% WO_3) between 1941 and 1957 (Krauskopf 1953). Of the Sierra Nevada tungsten mines, the CTM was among the top 20 producing mines by tonnage, although it was not one of the largest mines geographically (Newberry, 1980). The CTM skarn (11S 310960E, UTM 4056628N) formed in the aureole surrounding a 163 ± 1.5 Ma granodiorite pluton intruded into the northeastern tip of the Lake Kaweah pendant (Clemens-Knott et al. 2013). Based on mineral assemblages and chemistries, CTM skarn formation is estimated to have occurred at temperatures less than 700 °C, pressures of ~3-4 kbar, low X_{CO2}, and low fO_2 (Newberry 1980; Berekian 2008).

METHODS

Newberry (1980) mapped and described mineral assemblages defining the lithologic zonation within the CTM skarn. The mine is currently sealed, so samples of tremolite-diopside-epidote-quartz-garnet granofels, characteristic of the inner skarn, were collected with landowners permission from the tailings pile (Berekian 2008). Though tailings are expected to be poor in ore minerals, rare scheelite crystals surrounded by thin calcite rims were observed. Multiple grains of the unknown Ca-REE-Bi phosphate phases were first observed on high magnification backscatter electron (BSE) images of polished, carbon-coated thin sections under a ZEISS 1550VP field emission scanning electron microscope. Preliminary compositional data collected by SEM-energy dispersive spectroscopy identified the presence of the REEs Ce, La, Nd, and Pr;

Sm, Dy, Er and Yb, however, were not detected (abundances < one-sigma of 0.3 wt. %) so were not included in the subsequent analysis. Compositional data were collected using a JEOL 8200 electron microprobe (WDS: 15 kV; 25 nA; beam in focused mode) interfaced with the Probe for EPMA software. Possible interferences on peak position and background position were checked and corrected for all measured elements using the Probe for EPMA software. Standards for the analysis were anorthite (Ca*K*α, Al*K*α, Si*K*α), forsterite (Mg*K*α), fayalite (Fe*K*α), bismuth metal (Bi*M*α), ZnO (Zn*K*α), $CePO_4$ (P*K*α, Ce*L*α), $LaPO_4$ (La*L*α), GaAs (As*K*α), $PrPO_4$ (Pr*L*α), $NdPO_4$ (Nd*L*α), $GdPO_4$ (Gd*L*α), ThO_2 (Th*M*α), albite (Na*K*α), microcline (K*K*α), Mn_2SiO_4 (Mn*K*α), benitoite (Ba*L*α), anhydrite (S*K*α), tellurium metal (Te*L*α), and phlogopite (F*K*α). Quantitative elemental microanalyses were processed with the CITZAF correction procedure (Armstrong 1995).

Electron backscatter diffraction (EBSD) analysis was attempted with the goal of collecting structural data, using methods described in Ma and Rossman (2008, 2009). An HKL EBSD system on the Zeiss SEM was used and operated at 20 kV and 6 nA in a focused beam configuration with a 70º tilted stage and variable pressure (25 Pa) mode.

RESULTS

In the CTM skarn, the Ca-REE-Bi phosphates occur along grain boundaries between quartz and garnet, as members of replacement assemblages within the cores of zoned epidotes, and in anastomosing fractures that transect the coarse-grained crystals (Fig. 1a). Though tiny, the phosphate grains are easily recognized by their bright reflectance in BSE images (Fig. 1b). Nine acceptable microprobe analyses from two grains in a single sample contain higher atomic abundances of cerium (Ce) relative to lanthanum (La) (Table 1). REEs constitute up to 50 wt% of this phosphate: Ce_2O_3 contents range from 19.0 to 25.3 wt% (av. = 21.6 wt%) and La_2O_3

contents range from 14.0 to 18.8 wt% (av. = 16.8 wt%). In contrast to apatites (containing ~50-55 CaO wt.% and ~42 P_2O_5 wt.%), this phase contains only 5.8 to 8.3 wt% CaO (av. = 7.0 wt%) and only 18.9 to 28.4 wt% P_2O_5 (av. = 23.9 wt%). As much as 9.7 wt% As_2O_5 (av. = 2.9 wt%) substitutes for phosphorous. Calculating a hypothetical formula using 9 oxygens yields 5 cations; low EPMA totals and observed beam damage suggest the presence of either $(OH)_2$ or CO_3. Assuming the presence of hydroxyl yields a mean formula of $(Ca_{0.72}Ba_{0.06}Mg_{0.01})(Ce_{0.76}La_{0.60}Bi_{0.24}Nd_{0.20}Pr_{0.07}Al_{0.04}Mn_{0.02}Th_{0.02}Gd_{0.01}Fe_{0.01}Zn_{0.01})[(P_{1.94}As_{0.15})O_8](OH)_2$. A tenth analysis from a different sample has a similar composition, except that the atomic abundance of La (0.77) is greater than Ce (0.54; Table 2), consistent with the formula $(Ca_{0.84}Ba_{0.09}K_{0.01}Mg_{0.01})(La_{0.77}Ce_{0.54}Nd_{0.29}Pr_{0.15}Bi_{0.14}Th_{0.07}Gd_{0.01}Al_{0.01}Mn_{0.01}Fe_{0.01}Zn_{0.01})[(P_{1.99}As_{0.01})O_8](OH)_2$. Conversion of the average chemical compositions of these two phases into atomic abundances (atoms per formula unit, apfu; Tables 1, 2), and comparison of these results to the formula for apatite $[Ca_5(PO_4)_3(OH,F,Cl)]$ supports the following general formulas for these unknown phases: $CaCe_2[(P,As)O_4]_2(OH)_2$; $CaLa_2[(P,As)O_4]_2(OH)_2$. The theoretical total oxide weight percent that would be measured by electron microprobe for this hydroxyl-bearing phase is 96.69%, a total that is approached by the average of nine analyses (94.36 wt%; Table 1) and nearly equaled by a single analysis (96.21 wt%; Table 2). Alternatively, substituting CO_3 in the formula for hydroxyl yields a total hypothetical mass of ~104%. This unacceptably high total, coupled with the absence of excess carbon compared to other silicate phases analyzed in the same thin section, is most consistent with the inclusion of hydroxyl in the proposed formula.

Additional REE-rich phosphate grains were analyzed in samples of the CTM skarn, though quantitative data is currently insufficient to justify the designation of additional phases (Berekian 2008). This data is, however, useful in revealing details of compositional variations

within the REE-phosphates of the CTM skarn (Fig. 2). For example, the cation ratio of cerium to lanthanum appears to be positively correlated with the cation abundance of bismuth; specifically, the lanthanum decreases from 59 to 0% of the total (La + Ce) content as bismuth increases from 6 to 35% of the total (Bi + Ce + La). This relation suggests that bismuth (av. 9.4 wt%; range 4.1 to 16.1 wt%; Table 1) occupies the same lattice site as the REE.

EBSD analysis failed to yield useful structural data for the unknown Ca-REE-Bi phosphate phases. The high measured thorium contents (ThO_2 = 0-1.8 wt%; Table 1) suggest that the analyzed phases are now amorphous due to radiation damage (Farnen et al., 2007).

DISCUSSION

The potentially new Ca-REE-Bi phosphate minerals are members of assemblages that contain substantial concentrations of calcium (grossular garnet, diopsidic pyroxene, zoisite), phosphorus (both hydroxy-apatite and fluor-apatite) and the REE (ferriallanite) (Berekian 2008). A retrograde origin for the unknown Ca-REE-Bi phosphate phases is supported by their presence within secondary assemblages replacing the REE-rich ferriallanite cores of sector-zoned epidotes (Fig. 1a; Berekian 2008). Furthermore, the location of the unknown Ca-REE-Bi phosphate along potential pathways of fluid flow, such as fractures and grain boundaries, suggests a hydrothermal origin. This possibility is further supported by the spatial association of the unknown Ca-REE-Bi phosphate phases with the rare zeolite, brewsterite-Ba (Robinson and Grice 1993; Armbruster and Gunter 2001). The presence of this zeolite filling fractures and along grain boundaries suggests that the fracture-filling mineral assemblages formed at low temperatures during Stage 3 of skarn formation (Chipera and Apps 2001; Cabella et al. 1993), consistent with other reports of brewsterite-Ba in hydrothermal, low-temperature systems (Gottardi and Galli 1985; Green et al. 2005). Although the specific stability range of brewsterite-Ba is unknown, virtually all zeolites

form at <250°C in the presence of hydrothermal fluids (Chipera and Apps 2001). Other evidence suggestive of retrograde mineralization within the CTM skarn includes tremolite-calcite-quartz pseudomorphs of diopside (Berekian 2008). A detailed whole-rock oxygen isotope study demonstrates that the CTM skarn and the entire surrounding Stokes Mountain region did not experience subsequent hydrothermal events (Clemens-Knott, 1992).

Known REE-phosphate minerals include members from the monazite and apatite groups. For example, monazite-Ce has a comparable REE content to the unknown phase but does not contain calcium. Other monazite species, such as cheralite ($(Ca,Ce)(Th,Ce)(PO_4)_2$), contain calcium but do not contain hydroxyl. Hydroxy-apatites, such as britholite ($(Ca_2(Ce,Ca)_3(SiO_4,PO_4)_3(OH,F)$) and hydroxyl apatite ($Ca_5(PO_4)_3(OH)$), contain considerably more calcium. Substitution of SiO_4 for PO_4, as occurs in britholite, is not present in any of the potentially new phosphates observed in the CTM (Berekian 2008). Bismuth-bearing phosphates exist but the unknown phases reported herein appear to be the first reported, naturally occurring REE-bearing phosphates having high bismuth contents.

IMPLICATIONS

Mineralogic data from a quartz-garnet granofels collected from a Mesozoic calcsilicate skarn located in the western Sierra Nevada foothills suggests the discovery of at least two new phosphate phases having the compositions $Ca(Ce,La,Bi,Nd)_2[(P,As)O_4]_2(OH)_2$ and $Ca(La,Ce,Nd,Pr,Bi)_2[(P,As)O_4]_2(OH)_2$. Analyzed grains are too small and too metamict to support physical characterization. The presence of these unknown Ca-REE-Bi phosphate grains along cracks crosscutting the major silicates and within their replacement assemblages, coupled with the spatial association with the zeolite brewsterite-Ba, support formation of the unknown Ca-REE-Bi phosphate phases during the final stages of skarn formation. These results suggest

that detailed examination of fluid-flow pathways within retrograde skarn rocks may lead to the discovery of new mineral phases.

ACKNOWLEDGEMENTS

SEM, EBSD and EPMA analyses were carried out at the Caltech GPS Division Analytical Facility, which is supported, in part, by NSF Grants EAR-0318518 and DMR-0080065. Funding for this study was provided by a grant from the California State University system. Landowners of the Consolidated Tungsten Mine are thanked for providing access, and the Chrisman family is thanked for generous field support. Discussions with B. Browne, L. Meinert, R. Newberry, W. Nokleberg, J. Preston, J. Pyle, L. Robb, G. Rossman and F. Spear improved the content of this study, as did comments by Francis McCubbin and an anonymous reviewer.

REFERENCES CITED

Armbruster, T., and Gunter, M.E. (2001) Crystal structures of natural zeolites. In D.L. Bish, and D.W. Ming, Eds., Natural zeolites: Occurrence, properties, applications, 45, p. 1-67. Reviews in Mineralogy and Geochemistry, Mineralogical Society of America, Chantilly, Virginia.

Armstrong, J.T. (1995) CITZAF: A package of correction programs for the quantitative electron microbeam X-ray analysis of thick polished materials, thin films, and particles. Microbeam Analysis, 4, 177-200.

Berekian, B.J. (2008) A mineralogic study of the Consolidated Tungsten Mine skarn, Tulare County, California, 103 p. M.Sc. thesis, California State University, Fullerton.

Cabella, R., Lucchetti, G., Palenzona, A., Quartieri, S., and Vezzalini, G. (1993) First occurrence of Ba-dominant brewsterite: Structural features. European Journal of Mineralogy, 5, 353-360.

Chipera, S.J., and Apps, J.A. (2001) Geochemical stability of natural zeolites. In D.L. Bish, and D.W. Ming, Eds., Natural zeolites: Occurrence, properties, applications, 45, p. 117-161. Reviews in Mineralogy and Geochemistry, Mineralogical Society of America, Chantilly, Virginia.

Clemens-Knott, D. (1992) Geologic and isotopic investigations of the Early Cretaceous Sierra Nevada batholith, Tulare County, CA and the Ivrea Zone, NW Italian Alps: Examples of interaction between mantle-derived magma and continental crust, 349 p. Ph.D. thesis, California Institute of Technology, Pasadena, California.

Clemens-Knott, D., van der Kolk, D.A., Sturmer, D., and Saleeby, J. (2013) The Goldstein Peak Formation, central California: Record of a nonmarine intra-arc basin within the Early Cretaceous Sierra Nevada arc. Geosphere, 9, 718-735.

Corbett, G.J., and Leach, T.M. (1998) Southwest Pacific Rim gold-copper systems: Structure, alteration and mineralization, 238 p., Society of Economic Geologists, Special Publication 6, Bookcrafters, Chelsea, MI.

Einaudi, M.T., Meinert, L.T., and Newberry, R.J. (1981) Skarn deposits. In H.J. Skinner, Ed., 75th Anniversary Volume, p. 327-391. Society of Economic Geologists, Littleton, CO.

Farnen, I., Cho, H., and Weber, W., 2007, Quantification of actinide alpha-radiation damage in minerals and ceramics: Nature, v. 445, p. 190-193.

Gottardi, G., and Galli, E. (1985) Natural zeolites, 409 p. Springer-Verlag, Berlin.

211 Green, D.I., Tindle, A.G., and Moreton, S. (2005) Brewsterite-Ba and harmotome from the
212 Wicklow lead mines, Co. Wicklow, Ireland. Irish Journal of Earth Science, 23, 101-
213 106.
214 Jiao, M., Guo, N., Lu, W., Jia, Y., Lv, W., Zhao, Q., Shao, B., and You, H. (2013) Synthesis,
215 structure and photoluminescence properties of europium-, terbium-, and thulium-
216 doped $Ca_3Bi(PO_4)_3$ phosphors. Dalton Transactions, 42, 12395-12402.
217 Krauskopf, K.B. (1953) Tungsten deposits of Madera, Fresno, and Tulare Counties,
218 California, California Division of Mines Special Report 35, 83 p.
219 Kurtak, J.M. (2007) Mine in the Sky, 220 p. Bookcrafters, Chelsea, MI.
220 Ma, C. and Rossman, G.R. (2008) Barioperovskite, $BaTiO_3$, a new mineral from the Benitoite
221 Mine, California. American Mineralogist, 93, 154-157.
222 Ma, C. and Rossman, G.R. (2009) Tistarite, Ti_2O_3, a new refractory mineral from the Allende
223 meteorite. American Mineralogist, 94, 841-844.
224 Newberry, R.J. (1980) The geology and chemistry of skarn formation and tungsten
225 deposition in the central Sierra Nevada, California, 342 p. Ph.D. thesis, Stanford
226 University, California.
227 Newberry, R.J. (1982) Tungsten-bearing skarns of the Sierra Nevada: I, The Pine Creek
228 Mine, California. Economic Geology and the Bulletin of the Society of Economic
229 Geologists, 77, 823-844.
230 Newberry, R.J. (1998) W and Sn skarn deposits: A 1998 status report. In D.R. Lentz, Ed.,
231 Mineralized intrusion-related skarn systems, 26, p. 289-336. Short Course,
232 Mineralogical Society of Canada, Quebec.

Pan, Y., and Fleet, M. (2002) Compositions of the apatite-group minerals: Substitution mechanimsm and controlling factors. In M. Kohn, J. Rakovan, and J. Hughes, Eds., Phosphates: Geochemical, Geobiological, and Materials Importance, 48, p. 13-49. Reviews in Mineralogy and Geochemistry, Mineralogical Society of America, Chantilly, Virginia.

Robinson, G.W., and Grice, J.D. (1993) The barium analog of brewsterite from Harrisville, New York. The Canadian Mineralogist, 31, 687-690.

Spear, F., and Pyle, J. (2002) Apatite, monazite, and xenotime in metamorphic rocks. In M. Kohn, J. Rakovan, and J. Hughes, Eds., Phosphates: Geochemical, Geobiological, and Materials Importance, 48, p. 293-335. Reviews in Mineralogy and Geochemistry, Mineralogical Society of America, Chantilly, Virginia.

TABLE 1. Mean composition of Ce-dominant phase

Oxide	Ave. wt%	Range	apfu[a]
CaO	6.99(0.88)[b]	5.75-8.28	0.72
BaO	1.64(0.10)	1.46-1.76	0.06
K_2O	0.04(0.02)	0.00-0.06	0.00
ThO_2	0.77(0.53)	0.00-1.77	0.02
TeO_2	0.19(0.15)	0.00-0.52	0.01
MnO	0.22(0.18)	0.01-0.64	0.02
FeO	0.16(0.16)	0.00-0.49	0.01
MgO	0.06(0.02)	0.02-0.09	0.01
ZnO	0.19(0.08)	0.03-0.29	0.01
Ce_2O_3	21.64(1.99)	18.99-25.34	0.76
La_2O_3	16.76(1.54)	14.02-18.83	0.60
Bi_2O_3	9.37(3.44)	4.10-16.06	0.24
Pr_2O_3	2.04(0.36)	1.56-2.81	0.07
Nd_2O_3	5.92(0.76)	4.36-6.78	0.20
Gd_2O_3	0.40(0.13)	0.18-0.58	0.01
SiO_2	0.74(0.11)	0.57-0.87	0.07
Al_2O_3	0.37(0.13)	0.19-0.58	0.04
P_2O_5	23.89(3.26)	18.93-28.38	1.94
As_2O_5	2.92(3.85)	0.00-9.72	0.15
SO_3	0.05(0.02)	0.03-0.09	0.00
Total	94.36	--	4.94

[a] apfu: Atoms per formula unit based on 9 oxygen.
[b] Errors listed inside parentheses are one standard deviation of the mean based on nine analyses.

245

246

TABLE 2. Single analyses of Ce- and La-dominant phases

	Ce-dominant Phase		La-dominant Phase	
Oxide	(wt%)	(apfu[a])	(wt%)	(apfu)
CaO	6.73(0.03)	0.72	7.75(0.03)	0.84
BaO	1.46(0.07)	0.06	2.40(0.07)	0.09
K_2O	0.02(0.02)	0	0.05(0.01)	0.01
ThO_2	0.31(0.03)	0.01	2.91(0.04)	0.07
TeO_2	0.52(0.05)	0.02	b.d. [c]	
MnO	0.64(0.03)	0.05	0.06(0.03)	0.01
FeO	0.49(0.04)	0.04	0.13(0.03)	0.01
MgO	0.08(0.02)	0.01	0.05(0.01)	0.01
ZnO	0.10(0.05)	0.01	0.15(0.05)	0.01
Ce_2O_3	25.34(0.38)	0.92	14.67(0.29)	0.54
La_2O_3	14.02(0.34)	0.51	20.76(0.39)	0.77
Bi_2O_3	16.06(0.13)	0.41	5.36(0.08)	0.14
Pr_2O_3	1.77(0.09)	0.06	4.20(0.07)	0.15
Nd_2O_3	4.36(0.11)	0.16	8.05(0.13)	0.29
Gd_2O_3	0.25(0.07)	0.01	0.34(0.07)	0.01
SiO_2	0.83(0.02)	0.08	0.22(0.02)	0.02
Al_2O_3	0.47(0.02)	0.06	0.09(0.01)	0.01
P_2O_5	22.04(0.13)	1.85	23.35(0.14)	1.99
As_2O_5	0.64(0.23)	0.03	b.d.	
SO_3	0.09(0.01)	0.01	b.d.	
Total	96.21	5.02	90.54	4.97

[a] apfu: Atoms per formula unit based on 9 oxygen.
[b] Errors listed inside parentheses are 1-sigma of analytical error.
[c] b.d. = Below detection limit: 0.07 wt% Te, 0.28 wt% As and 0.01 wt% S.

247

FIGURE CAPTIONS

Figure 1. BSE images of the unknown Ca-REE-Bi phosphate phase: (a) sector-zoned REE-bearing epidote crystal with altered REE-rich core composed of an assemblage of REE-bearing epidote-family minerals (shades of gray) crosscut by the unknown Ca-REE-Bi phosphate phase (white); (b) bright grain located along a grain boundary between garnet (left) and quartz (right).

Figure 2. Ternary plot displaying the relative atomic abundances of calcium, bismuth and the analyzed REE (Ce + La + Pr + Nd). Symbols: Ce-dominant Ca-REE-Bi phosphate (open triangles); La-dominant Ca-REE-Bi phosphate (solid square); as many as four additional and distinct unknown REE-phosphate phases (crosses; Berekian 2008). Note: lanthanum contents were not measured for the three samples (crosses) that plot on the Ce-Bi tie-line.

This is a preprint, the final version is subject to change, of the American Mineralogist (MSA)
Cite as Authors (Year) Title. American Mineralogist, in press.
(DOI will not work until issue is live.) DOI: http://dx.doi.org/10.2138/am-2015-4960

Berekian_Fig1a

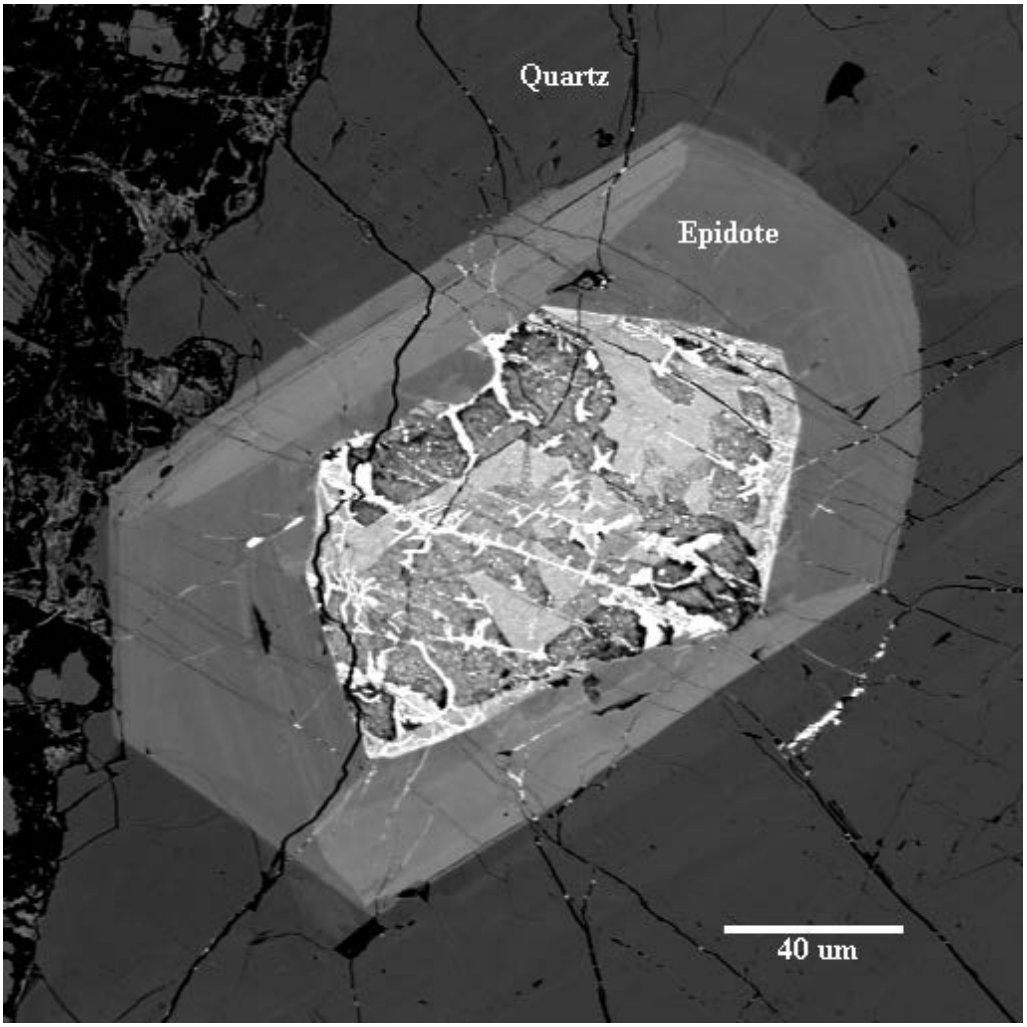

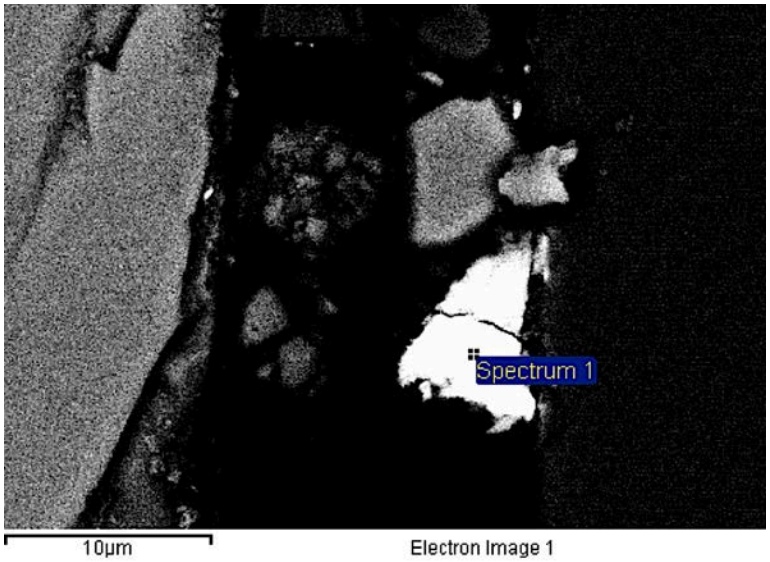

Berekian_Fig2.ai